

Galaxy assembly bias of central galaxies in the Illustris simulation

Xiaoju Xu[★] and Zheng Zheng[†]

Department of Physics and Astronomy, University of Utah, 115 South 1400 East, Salt Lake City, UT 84112, USA

Accepted XXX. Received YYY; in original form ZZZ

ABSTRACT

Galaxy assembly bias, the correlation between galaxy properties and halo properties at fixed halo mass, could be an important ingredient in halo-based modelling of galaxy clustering. We investigate the central galaxy assembly bias by studying the relation between various galaxy and halo properties in the Illustris hydrodynamic galaxy formation simulation. Galaxy stellar mass M_* is found to have a tighter correlation with peak maximum halo circular velocity V_{peak} than with halo mass M_h . Once the correlation with V_{peak} is accounted for, M_* has nearly no dependence on any other halo assembly variables. The correlations between galaxy properties related to star formation history and halo assembly properties also show a cleaner form as a function of V_{peak} than as a function of M_h , with the main correlation being with halo formation time and to a less extent halo concentration. Based on the galaxy-halo relation, we present a simple model to relate the bias factors of a central galaxy sample and the corresponding halo sample, both selected based on assembly-related properties. It is found that they are connected by the correlation coefficient of the galaxy and halo properties used to define the two samples, which provides a reasonable description for the samples in the simulation and suggests a simple prescription to incorporate galaxy assembly bias into the halo model. By applying the model to the local galaxy clustering measurements in Lin et al. (2016), we infer that the correlation between star formation history or specific star formation rate and halo formation time is consistent with being weak.

Key words: galaxies: haloes – galaxies: statistics – cosmology: theory – large-scale structure of Universe

1 INTRODUCTION

It has been well established that galaxies form in dark matter haloes (White & Rees 1978). As the first step to study galaxy formation and clustering, halo formation and clustering, which is dominated by gravity, have been extensively studied with analytic models (e.g. Press & Schechter 1974; Barden et al. 1986; Mo & White 1996; Sheth & Tormen 1999) and cosmological N -body simulations (e.g. Springel 2005; Prada et al. 2012). It has been found that halo clustering depends not only on halo mass but also on halo assembly history and environment (e.g. Gao et al. 2005; Gao & White 2007; Paranjape et al. 2018; Xu & Zheng 2018; Han et al. 2019; Ramakrishnan et al. 2019), or halo definition (e.g. Villarreal et al. 2017; Mansfield & Kravtsov 2019). This is called halo assembly bias, whose nature is still under inves-

tigation (e.g. Dalal et al. 2008; Castorina & Sheth 2013; Shi & Sheth 2018).

If galaxy properties are affected by halo formation and assembly history, halo assembly bias would translate to galaxy assembly bias. Operationally, galaxy assembly bias can be defined as that at fixed halo mass, the statistical galaxy content shows dependence on other halo variables or galaxy properties show correlations with halo assembly history (which would cause a certain degree of halo assembly bias to be inherited by galaxies and to show up in galaxy clustering). The widely adopted halo model (e.g. Cooray & Sheth 2002) of interpreting galaxy clustering, such as the halo occupation distribution (e.g., Berlind & Weinberg 2002; Zheng et al. 2005) or conditional luminosity function (e.g., Yang et al. 2003), makes the implicit assumption of no galaxy assembly bias. Such methods have been successfully applied to galaxy clustering (e.g. Zehavi et al. 2005; Zheng et al. 2007; Xu et al. 2018). However, if assembly bias is significant, neglecting it in the model would lead to in-

[★] E-mail: xiaoju.xu@utah.edu

[†] E-mail: zhengzheng@astro.utah.edu

correct inference of galaxy-halo connections and introduce possible systematics in cosmological constraints (e.g. Zentner et al. 2014, 2019; but see also McEwen & Weinberg 2016; McCarthy, Zheng & Guo 2019). Conversely, observationally inferred galaxy assembly bias would help understand galaxy formation.

The existence and strength of galaxy assembly bias are still a matter far from settled, either in theory or in observation. Galaxy assembly bias has been investigated in hydrodynamic (e.g. Berlind et al. 2003; Mehta 2014; Chaves-Montero et al. 2016; Artale et al. 2018; Martizzi et al. 2019; Bose et al. 2019) or semi-analytic galaxy formation models (e.g. Croton et al. 2007; Contreras et al. 2019; Zehavi et al. 2018, 2019), focusing on the effect on galaxy occupation function and galaxy clustering. The results seem to depend on the implementation details of star formation and feedback. Studying galaxy assembly bias from observation has the difficulty of determining halo mass, and the results are not conclusive (e.g. Yang et al. 2006; Berlind et al. 2006; Lin et al. 2016; Zu et al. 2017; Guo et al. 2017). Given the potential importance of galaxy assembly bias in modelling galaxy clustering, in this paper we study the correlation between various central galaxy properties and halo properties in the Illustris hydrodynamic simulation (Vogelsberger et al. 2014a) at the halo level, aiming at providing useful insights in describing galaxy assembly bias.

The structure of the paper is as follows. In section 2, we introduce the simulation and the galaxy and halo catalogues. Then in section 3, we investigate the relation between galaxy and halo properties, with primary galaxy-halo properties in section 3.1 and general galaxy-halo properties in section 3.2. In section 3.3, we present a simple model to connect galaxy assembly bias with halo assembly bias. Finally, we summarise and discuss the results in section 4.

2 SIMULATION AND GALAXY-HALO CATALOGUE

In this work, we use galaxies and haloes from the state-of-the-art hydrodynamic galaxy formation simulation Illustris¹ (Vogelsberger et al. 2014a; Nelson et al. 2015) to study galaxy assembly bias, which is able to produce different type of galaxies seen in observation (Vogelsberger et al. 2014b; Genel et al. 2014). In particular, we use the Illustris-2 simulation, which has a box size of $75h^{-1}\text{Mpc}$ on a side, and contains 910^3 dark matter particles of mass $5 \times 10^7 M_\odot$ and the same number of baryon particles of mass $1 \times 10^7 M_\odot$. The mass resolution is sufficient for our purpose of studying (central) galaxies in haloes of more massive than a few times $10^{10} h^{-1} M_\odot$. The simulation adopts a spatially-flat cosmology with the following parameters: $\Omega_m = 0.27$, $\Omega_b = 0.0456$, $h = 0.70$, $n_s = 0.963$, and $\sigma_8 = 0.809$.

The haloes in the Illustris database are identified with the friends-of-friends (FoF) algorithm. As this algorithm is notorious for having the probability of bridging two separate halos into one halo, we apply the phase-space halo finder Rockstar (Behroozi et al. 2013a) to identify haloes, with dark matter particles extracted from 30 snapshots of

the simulation (from $z=3.94$ to $z=0$). We then build the merger tree using the consistent-tree algorithm (Behroozi et al. 2013b).

We focus our study on the relation between central galaxies and dark matter haloes and the assembly effect at $z = 0$. Galaxies in the Illustris-2 simulation are assigned to the Rockstar haloes. For each galaxy, if its distance d_{gh} to the centre of a halo is smaller than the virial radius R_{vir} of the halo, it is assigned to this halo. In rare cases, a galaxy may be assigned to more than one haloes, as haloes are not spherical. We then put the galaxy into the halo that corresponds to the lowest ratio of d_{gh}/R_{vir} . With galaxies assigned to haloes, for each halo we define the most massive galaxy inside $0.2R_{\text{vir}}$ from the halo centre to be the central galaxy. If there is no galaxy inside $0.2R_{\text{vir}}$, we simply choose the most massive galaxy inside R_{vir} as the central galaxy.

With the catalogue of central galaxies and the associated host haloes, we study the relation between galaxy properties and halo properties and the assembly effects. The halo properties we focus on are:

- (1) M_h , halo mass enclosed in a volume with mean density of 200 times the background density of the universe;
- (2) V_{peak} , peak maximum circular velocity of the halo over its accretion history;
- (3) c , halo concentration parameter, defined as the ratio of halo virial radius to scale radius;
- (4) $a_{M/2}$, cosmic scale factor when the halo obtains half of its current ($z = 0$) total mass;
- (5) \dot{M}_h , halo mass accretion rate near $z = 0$ (averaged between $z=0$ and $z=0.197$, about 2.4 Gyr, one dynamical time), in units of $h^{-1} M_\odot \text{yr}^{-1}$;
- (6) \dot{M}_h/M_h , specific halo accretion rate, in units of Gyr^{-1} .

The central galaxy properties we consider include:

- (1) M_* , stellar mass (sum of masses of star particles within twice the stellar half mass radius);
- (2) SFR, star formation rate within twice the stellar half mass radius;
- (3) sSFR, specific star formation rate, the ratio of SFR to M_* ;
- (4) $g - r$, galaxy colour defined by the g -band and r -band luminosity.

3 RESULTS

We aim at presenting the relation between central galaxies and haloes to learn about the correlation between halo formation and assembly and galaxy properties. In section 3.1 We first study how galaxy stellar mass depends on the primary halo properties (M_h and V_{peak}). Then we investigate how various halo and galaxy properties are correlated in section 3.2. Finally, in section 3.3 we use a simplified model to describe the connection between galaxy and halo assembly bias factor.

3.1 Relationship between stellar mass and halo properties

Galaxy stellar mass is a primary property inferred from observation. The relation between this primary galaxy property and certain primary halo property (e.g., M_h and V_{peak})

¹ <http://www.illustris-project.org>

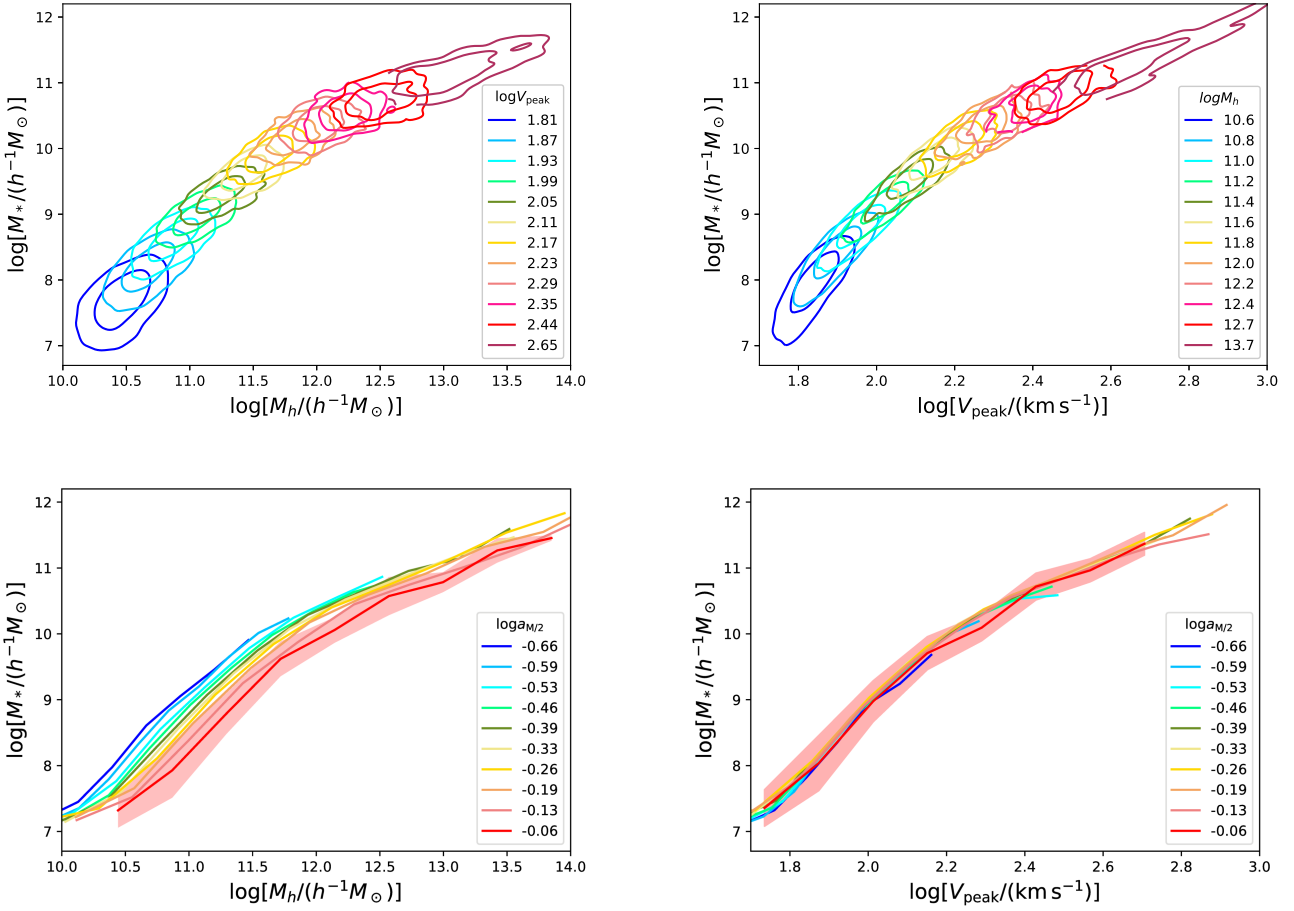


Figure 1. Top-left: M_* as function of M_h for central galaxies. The galaxies are colour-coded according to $\log[V_{\text{peak}}/(\text{km s}^{-1})]$. For galaxies in each bin of $\log V_{\text{peak}}$, the contours correspond to the 68.3 and 95.4 per cent distribution, respectively. Top-right: M_* as function of V_{peak} for central galaxies, colour coded according to the values of $\log[M_h/(h^{-1}M_\odot)]$. Bottom-left: M_* as function of M_h for central galaxies, with the mean relation colour-coded according to the values of $a_{M/2}$. For clarity, the scatter in the mean relation is only shown for the bin with the highest $a_{M/2}$ (latest forming haloes). Bottom-right: M_* as function of V_{peak} for central galaxies, colour-coded according to $a_{M/2}$, with the shaded region illustrating the scatter for the bin with the highest $a_{M/2}$. Note the remarkable result that M_* does not depend on $a_{M/2}$ at fixed V_{peak} (compared to the M_h case in the bottom-left panel).

can be established based on subhalo abundance matching or modelling the stellar mass dependent clustering, which encodes information about galaxy formation. Here we show the relation predicted by the Illustris simulation and study how tight stellar mass correlates with M_h and V_{peak} .

The top-left panel of Fig. 1 shows M_* as function of M_h , colour-coded with values of V_{peak} . Galaxy stellar mass M_* increases steeply with M_h at $\log[M_*/(h^{-1}M_\odot)] < 12$ and then slowly at $\log[M_*/(h^{-1}M_\odot)] > 12$, a trend similar to that inferred from observation (e.g. Behroozi et al. 2010; Leuthaud et al. 2012; Zu & Mandelbaum 2015). The scatter in M_* at fixed halo mass in the M_*-M_h relation decreases with increasing M_h (solid curve in Fig. 2), varying from about 0.3 dex at the low-mass end to about 0.17 dex at the high-mass end. The scatter at the high-mass end is consistent with the value ~ 0.16 dex inferred from galaxy clustering modelling (e.g. Tinker et al. 2017). One source of the scatter can be the halo formation history (Tinker 2017), which may affect the growth history of stellar mass (either from star formation or galaxy merging; e.g. Gu et al. 2016).

The colour code in V_{peak} in the top-left panel enables us to see how the scatter in the M_*-M_h relation may be connected to halo assembly. On average, V_{peak} and M_h are correlated, and the mean relation is found to be well described by

$$V_{\text{peak}} = 170 \left(\frac{M_h}{10^{12} h^{-1} M_\odot} \right)^{1/3} \text{ km s}^{-1} \quad (1)$$

in the Illustris simulation. However, there is scatter on top of the mean relation, and at fixed M_h , the distribution of V_{peak} reflects that in the assembly history. As can be seen in the top-left panel, the assembly of haloes encoded in V_{peak} does contribute to the scatter in the M_*-M_h relation – at fixed M_h , galaxies residing in haloes of higher V_{peak} tend to have higher stellar mass, especially at the low mass end.

To see how well the scatter in M_* can be attributed to the scatter in V_{peak} , in the top-right panel of Fig. 1, we plot the M_*-V_{peak} relation. It follows a similar trend seen in the M_*-M_h relation, steeper (shallower) dependence of M_* on V_{peak} at the low (high) V_{peak} end, which is expected given

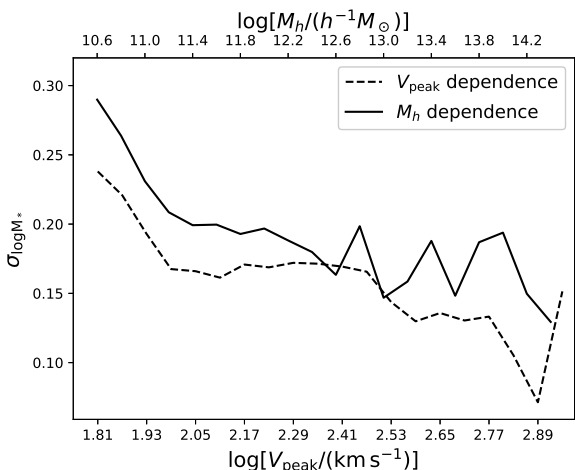


Figure 2. Standard deviation in $\log M_*$ as a function of M_h (solid) and V_{peak} (dashed). The correspondence between M_h and V_{peak} is from the mean relation $V_{\text{peak}} \propto M_h^{1/3}$ in equation (1). Poisson errors in $\log M_*$ caused by finite number of star particles have been subtracted in quadrature.

the correlation between V_{peak} and M_h . The M_* - V_{peak} relation appears to be tighter than the M_* - M_h relation, in the sense that at fixed V_{peak} the scatter in M_* is lower than that at the corresponding M_h (see [Matthee et al. 2017](#) for a similar result in terms of $z = 0$ maximum halo circular velocity with the EAGLE simulation). The scatter varies from ~ 0.28 dex at low V_{peak} to ~ 0.13 dex at high V_{peak} (dashed curve in Fig. 2). In the M_* - V_{peak} plot (top-right panel), the contours are colour-coded by M_h . Unlike the M_h case in the top-left panel, we find that M_* does not show a clear dependence on M_h – at fixed V_{peak} (i.e. by taking a vertical cut in the plot), M_* in haloes of different M_h appears to follow similar mean and scatter.

In the bottom-left panel, we show the effect of the other halo assembly property $a_{M/2}$ on the M_* - M_h relation. Each curve show the mean M_* - M_h relation for haloes in one $a_{M/2}$ bin. The scatter around the mean relation is illustrated with the shaded region, only shown for the latest forming haloes to avoid crowdedness. There is a clear and substantial dependence of the M_* - M_h relation on the assembly property $a_{M/2}$ – at fixed M_h , haloes forming earlier (smaller $a_{M/2}$) tend to host galaxies of higher M_* . Such a trend is consistent with previous work based on the EAGLE simulation ([Matthee et al. 2017](#)) and semi-analytic galaxy formation model ([Zehavi et al. 2018](#)).

Switching to the M_* - V_{peak} relation (bottom-right panel), we find that at fixed V_{peak} there is no dependence of M_* on the assembly property $a_{M/2}$, with the curves of different $a_{M/2}$ bins all falling on top of each other. As further shown in section 3.2, V_{peak} is able to absorb the effect on M_* from any other halo assembly variable. This is consistent with the results using $z = 0$ maximum halo circular velocity ([Matthee et al. 2017](#)). We will discuss this remarkable result in section 4.

The other commonly adopted halo circular velocity quantity is V_{max} , the present-day maximum circular velocity of a halo. In Appendix A, we show that the M_* - V_{max} relation is similar to the M_* - V_{peak} relation, but with the former

showing a little bit residual dependence on halo formation time. In Appendix A, by replacing V_{peak} used here from the full physics simulation with the one from the dark-matter-only simulation, we also show that baryon effect on the halo potential plays almost no role in driving V_{peak} to track M_* .

The tighter correlation between M_* - V_{peak} , in comparison to M_* - M_h , suggests that in galaxy clustering modelling galaxy assembly bias effect can be partially account for by switching from a M_h -based model to a V_{peak} -based model. That is, the galaxy-halo relation is parameterised as a function of V_{peak} . This is in line with the finding by [Chaves-Montero et al. \(2016\)](#) using the EAGLE simulation, while their velocity quantity most strongly correlating with M_* is slightly different, V_{relax} , the highest value of the maximum circular velocity of a subhalo with a relaxation criterion imposed. [Chaves-Montero et al. \(2016\)](#) show that V_{relax} is able to capture the majority (but not all) of the galaxy assembly bias effect on galaxy clustering for stellar-mass-based samples. The tighter correlation between M_* - V_{peak} may also be the reason that when using subhalo abundance matching or its variants to model galaxy clustering, halo circular velocity-based models usually have good performances (e.g. [Reddick et al. 2013](#); [Guo et al. 2016](#)).

To investigate how well assembly bias effect in Illustris central galaxy clustering can be absorbed by V_{peak} , we perform a test by constructing shuffled galaxy catalogues (e.g. [Croton et al. 2007](#); [Zu, Zheng, Zhu & Jing 2008](#)) and compare the two-point correlation functions of the original and shuffled central galaxy samples, selected by stellar mass thresholds. By dividing haloes into small V_{peak} bins, we randomly shuffle the values of M_* among haloes in each V_{peak} bin, which eliminates the dependence of M_* on halo properties other than V_{peak} . If V_{peak} can account for all assembly effects on central galaxy M_* , we would expect the V_{peak} -shuffled sample to have the same two-point correlation function as the original, unshuffled sample. For comparison, we also similarly construct V_{max} -shuffled and M_h -shuffled samples. In the left panel of Fig. 3, the result is shown for the $\log[M_*/(h^{-1}M_\odot)] > 9$ sample. The M_h -shuffled sample show the largest deviation in the two-point correlation function from the original sample, with the assembly effect on galaxy clustering at a level of 10 per cent. The level of deviation is small (below ~ 2 per cent on most scales above $1h^{-1}\text{Mpc}$) for the V_{peak} -shuffled sample, suggesting that V_{peak} is able to absorb the majority of the assembly bias on stellar mass. The result with the V_{max} -shuffled sample is in between, and V_{max} is not as efficient as V_{peak} in absorbing the assembly bias effect on stellar mass (consistent with that seen in Appendix A). For the $\log[M_*/(h^{-1}M_\odot)] > 10$ sample (right panel), the assembly bias effect is also at the 10 per cent level, and both V_{peak} and V_{max} are able to roughly absorb more than half of it, with V_{peak} behaving marginally better than V_{max} . We note that the overall trend is similar to that in [Zehavi et al. \(2019\)](#) based on galaxies in a semi-analytic galaxy formation model (top panel of their fig.8 for central galaxies). As a whole, we see that V_{peak} is able to absorb a large fraction of the assembly effect on central galaxy stellar mass, more efficient for lower mass haloes, suggesting that V_{peak} may serve as a good halo variable to replace M_h in modelling clustering of galaxies selected by stellar mass.

In what follows, besides a further investigation of the

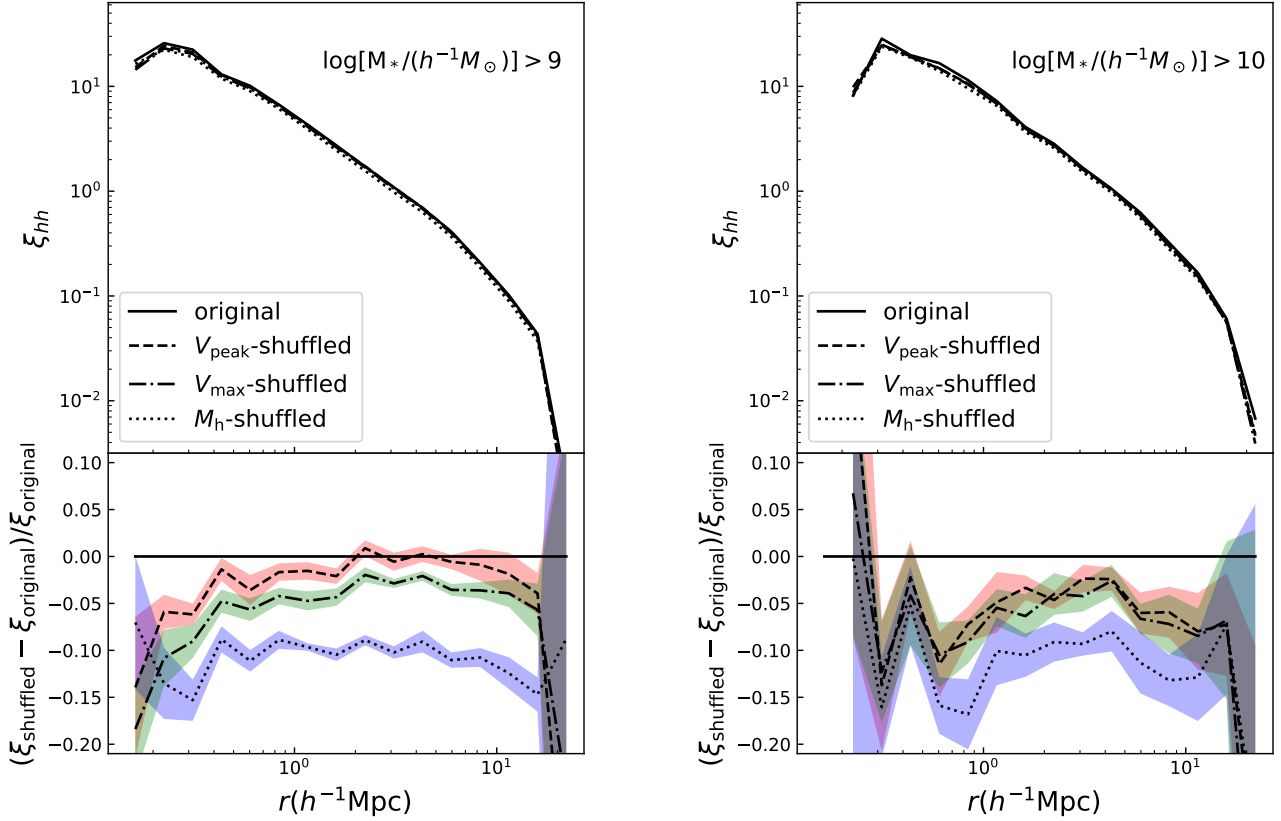


Figure 3. Comparison of two-point correlation functions of original and shuffled central galaxy samples, selected by stellar mass thresholds. Left: The top panel compares the two-point correlation functions of central galaxies with $\log[M_*/(h^{-1}M_\odot)] > 9$ from the original, unshuffled sample (solid) and the $M_h/V_{\text{max}}/V_{\text{peak}}$ -shuffled samples (dotted/dot-dashed/dashed). The bottom panel shows fractional differences between those from the shuffled and original samples, with each shaded band indicating the uncertainty estimated from 10 shuffling realisations. Right: same as the left, but for central galaxy samples with $\log[M_*/(h^{-1}M_\odot)] > 10$. See details in section 3.1.

dependence of stellar mass on halo assembly variables, we also extend the study to other galaxy properties.

3.2 Relationship between galaxy properties and halo properties

With the 7 halo properties (M_h , V_{peak} , c , $a_{M/2}$, λ , \dot{M}_h , and \dot{M}_h/M_h) and the 4 central galaxy properties (M_* , SFR, sSFR, and $g-r$ colour), we study the correlations between them. To aid the discussion, we also present the correlations among halo properties and those among galaxy properties.

3.2.1 At fixed M_h

Fig. 4 shows the correlation between each pair of the halo and galaxy properties for central galaxies in haloes of a narrow mass bin, $\log[M_h/(h^{-1}M_\odot)] = 12.0 \pm 0.1$. In each contour panel, the contours indicate the 68.3 and 95.4 per cent of the distribution of the pair of properties. The number labelled

in each panel is the Pearson correlation coefficient ρ of the two properties, indicating how strong the correlation is. It is calculated as

$$\rho = \frac{\langle xy \rangle - \langle x \rangle \langle y \rangle}{\sigma_x \sigma_y}, \quad (2)$$

where x and y denote the two properties, $\langle \rangle$ means average, and σ_x and σ_y are the standard deviations of x and y . The panel at the top of each column shows the marginalised distribution of the property labelled at the x -axis of the column.

The panels with red contours (i.e. the top 6 rows and left 6 columns of contour panels) display the correlation between halo properties. Within the small but finite halo mass bin, all but one halo property shows almost no correlation with M_h (correlation coefficient close to zero). The exception is V_{peak} , and the correlation is simply driven by the $V_{\text{peak}} \propto M_h^{1/3}$ mean relation. At fixed M_h , any pair of halo properties show a substantial correlation (with $|\rho|$ above 0.2). The nearly perfect correlation ($\rho = 0.983$) between \dot{M}_h and \dot{M}_h/M_h is a

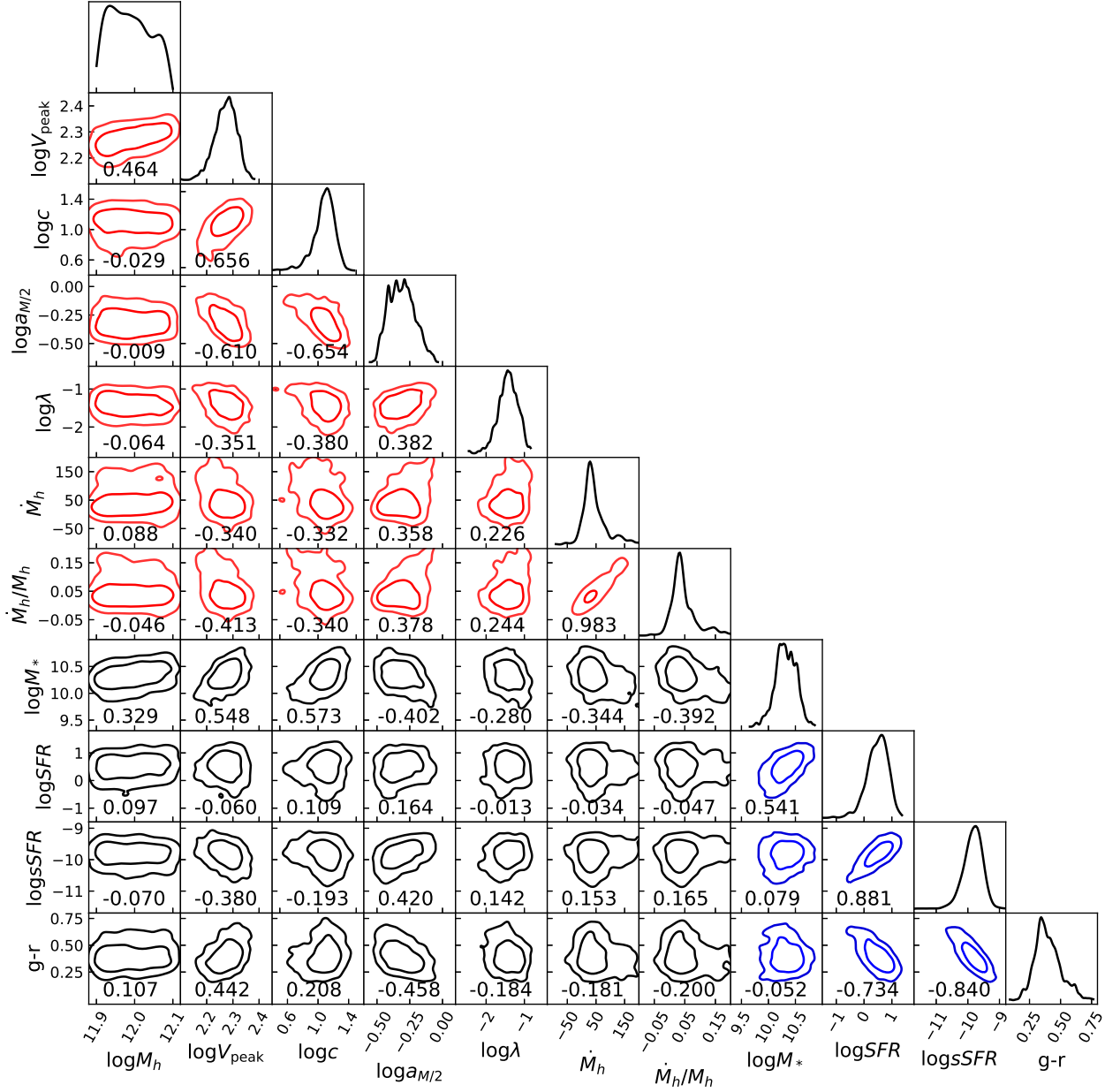


Figure 4. Relation between each pair of galaxy and/or halo properties at $\log[M_h/(h^{-1}M_\odot)] \sim 12$. In each contour panel, the two contours show the central 68.3 and 95.4 per cent of the distribution of the pair of properties. The panels with red contours (i.e. the top 6 rows and left 6 columns of contour panels) display the correlations between halo properties. Those with black contours (i.e. the bottom 4 rows and left 7 columns of contour panels) show the correlations between galaxy and halo properties, and those with blue contours (i.e. the right 3 columns of contour panels) are for the correlations between pairs of galaxy properties. The number in each contour panel is the Pearson correlation coefficient for the pair of properties. The histogram at the top panel of each column is the probability distribution function of the variable of that column.

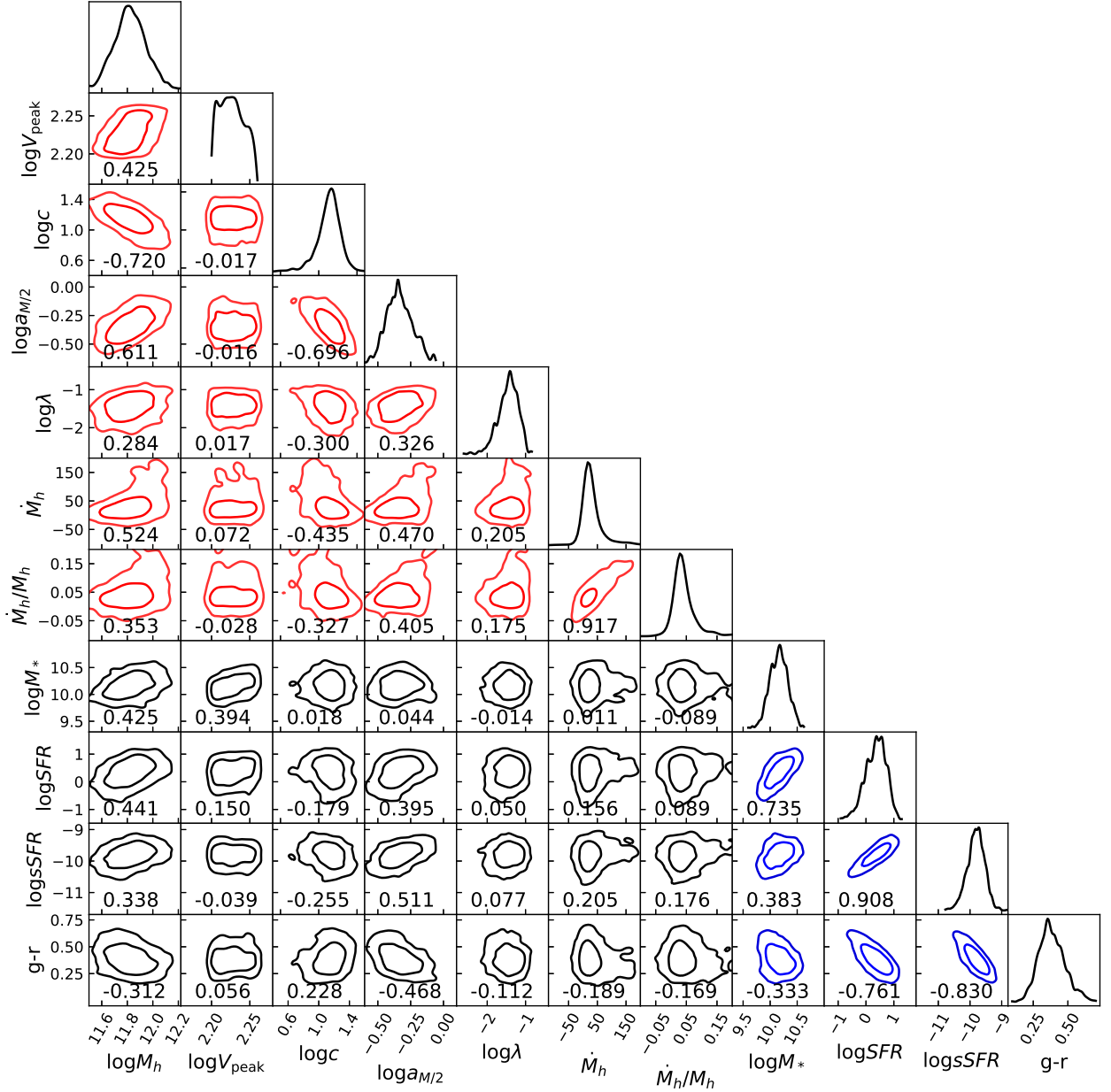


Figure 5. Same as Fig. 4, but at fixed $\log[V_{\text{peak}}/(\text{km s}^{-1})] \sim 2.23$. Note particularly the lack of correlation of M_* with other assembly variables (including c , $a_{M/2}$, λ , M_h , M_h/M_h), in contrast with the case in Fig. 4.

consequence of fixed M_h . Overall the correlation trend is that haloes of higher V_{peak} are more concentrated, form earlier, spin more slowly, and have lower accretion rate, which have been seen in previous work (e.g. [Jeon-Daniel et al. 2011](#); [Han et al. 2019](#); [Xu & Zheng 2018](#)).

The panels with black contours (i.e. the bottom 4 rows and the left 7 columns of contour panels) show the corre-

lation between halo and galaxy properties. The correlation between M_* and M_h shows up because of the finite size of the halo mass bin. At fixed M_h , the central galaxy stellar mass M_* correlates with all other halo properties – haloes of higher V_{peak} , higher concentration, earlier formation, lower spin, and lower accretion rate tend to host more massive central galaxies. On the contrary, the SFR shows no strong cor-

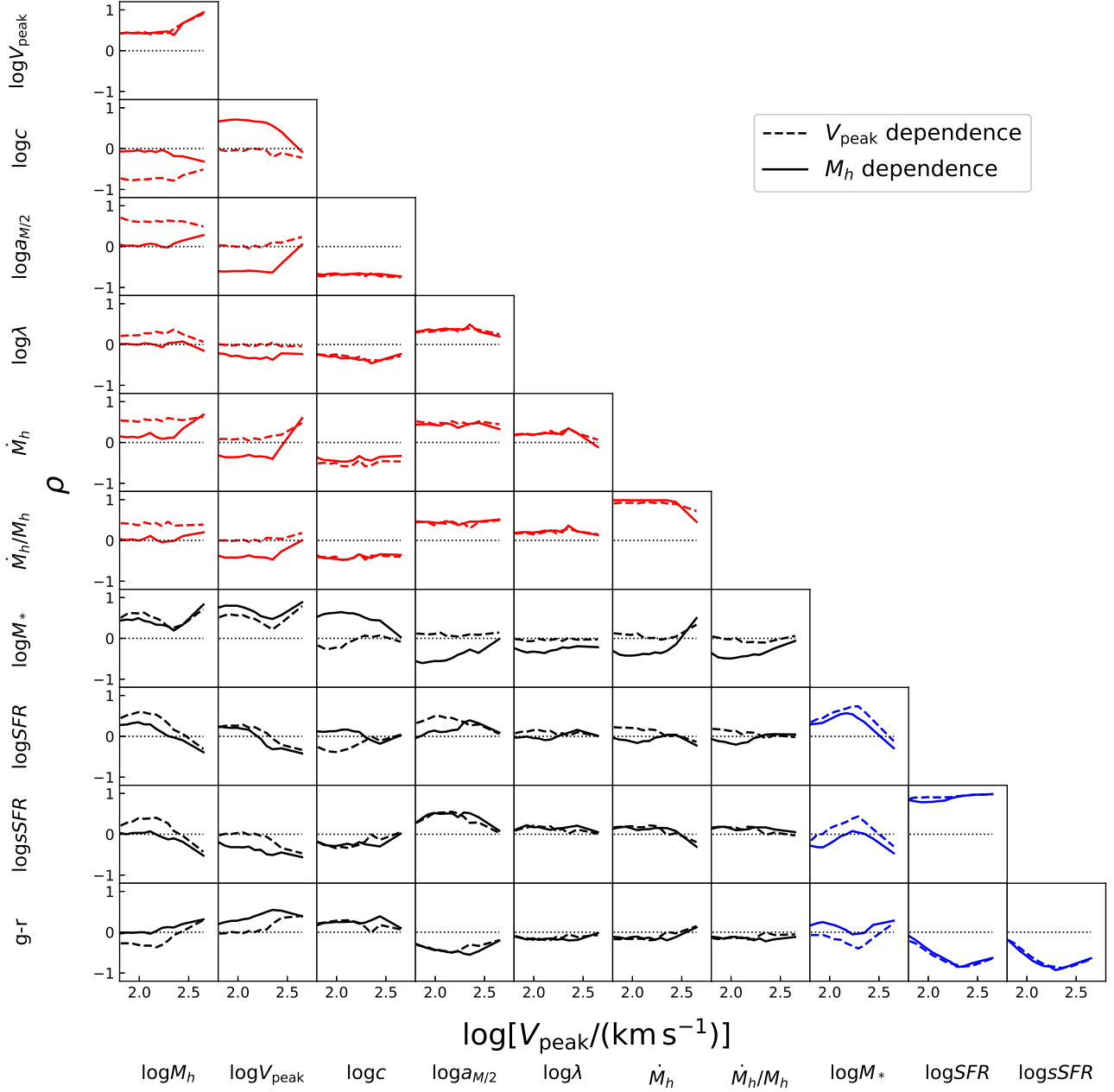


Figure 6. Pearson correlation coefficient ρ of each pair of galaxy and/or halo properties as a function of M_h (solid) and V_{peak} (dashed). The galaxy and halo properties are marked to the far left of each row and at the bottom of each column. For clarity, we only label the values of V_{peak} on the horizontal axis, and the values of M_h can be inferred from $M_h \propto V_{\text{peak}}^3$ from equation (1). As with Fig. 4, panels with red, black, and blue curves are for correlations between halo-halo, galaxy-halo, and galaxy-galaxy properties, respectively. In each panel, the dotted horizontal line indicates no correlation. Note particularly the lack of correlation of M_* with other assembly variables (including c , $a_{M/2}$, λ , \dot{M}_h , \dot{M}_h/M_h) for the V_{peak} dependence case, in contrast with the M_h dependent case. Also the correlations of SFR, sSFR, and colour with halo assembly variables show more consistent behaviours in the V_{peak} dependence case.

relation with any halo properties. The most significant one is with halo formation time ($\rho \sim 0.16$), with on average higher SFR in haloes of later formation. Given the substantial correlation between M_* and halo properties and the weak or lack of correlation between SFR and halo properties, the sSFR ($\equiv \text{SFR}/M_*$) is expected to correlate well with halo properties, but in a trend opposite to and weaker than that with M_* . This is indeed the case. The most significant correlation is with V_{peak} or $a_{\text{M}/2}$ (both with $|\rho| \sim 0.4$). The correlation between sSFR and the average halo accretion rate over the past dynamic time is there but not strong ($\rho \sim 0.16$). The correlation between galaxy colour $g-r$ and halo properties essentially follows the case of sSFR (with a sign change in ρ ; redder galaxies having lower sSFR).

The panels with blue contours (i.e. the right 3 columns of contour panels), the correlations between pairs of galaxy properties at fixed halo mass are shown. The SFR positively correlates with M_* ($\rho \sim 0.54$), and the mean relation has a slope close to unity, $\text{SFR} \propto M_*$. It resembles the star-forming main sequence (e.g. Brinchmann et al. 2004; Speagle et al. 2014; Santini et al. 2017). That is, even if we only consider central galaxies in haloes of fixed mass, the star-forming main sequence emerges. Note that this SFR– M_* correlation is not driven by the correlation of SFR and M_* with a common halo variable we consider here. In fact, from Fig. 4, it can be seen that their correlation with a common halo variable may lead to the opposite effect. For example, haloes of earlier formation tend to host central galaxies of higher M_* and lower SFR, and naively this would imply an anti-correlation between SFR and M_* , opposite to what is found here. While it is possible that the halo-level star-forming main sequence is related to a halo variable not considered here, it is more likely that the sequence is driven by baryonic physics, which may have complicated dependence on or decouple from halo formation history. Unlike the SFR, the sSFR shows little dependence on M_* . However, the sSFR is tightly correlated with the SFR ($\rho \sim 0.88$). Given that $\text{sSFR} \equiv \text{SFR}/M_*$, the pattern in the mutual correlations among M_* , SFR, and sSFR can be achieved if the SFR– M_* correlation coefficient is close to the ratio of the scatters in $\log M_*$ and $\log \text{SFR}^2$, which appears to be the case. Galaxy $g-r$ colour strongly correlates with sSFR and follows the same trends as sSFR in its correlations with M_* and SFR.

Overall, at fixed halo mass, galaxy properties other than SFR show significant correlations with one or more halo properties, manifesting galaxy assembly bias at the level of haloes. The correlations among galaxy properties, however, may largely result from baryonic physics, given that the trend cannot be simply explained by their correlation with halo properties. In section 3.1, it is found that switching from M_{h} to V_{peak} can remove the dependence of M_* on other halo properties. We now extend the investigation to other galaxy properties.

3.2.2 At fixed V_{peak}

Fig. 5 is similar to Fig. 4, but the correlations are presented for haloes at a fixed V_{peak} bin, $\log[V_{\text{peak}}/(\text{km s}^{-1})] = 2.23 \pm 0.03$. The correlations among halo properties (in panels with red contours) are similar to those in Fig. 4, and there are additional correlations between M_{h} and other halo properties.

The galaxy-halo correlations are shown in panels with black contours. The finite bin size in V_{peak} makes the M_* – V_{peak} correlation show up. Other than this (and the one with M_{h}), M_* does not correlate with any other halo properties at fixed V_{peak} , reinforcing the result in section 3.1. It indicates that the correlations of M_* with halo properties seen at fixed M_{h} (Fig. 4) can be attributed to the M_* – V_{peak} correlation and the correlation of V_{peak} with other halo properties. For the SFR, at fixed V_{peak} , it correlates significantly with M_{h} and $a_{\text{M}/2}$, higher SFR in haloes of higher mass and later formation. The correlations between SFR and other halo properties are weak. The correlations between sSFR (or colour) and halo properties closely follow the SFR case.

In terms of the galaxy-galaxy correlations, the trends are similar to those seen at fixed halo mass, except that the sSFR and colour now show clear correlations with M_* .

As a whole, using V_{peak} as the halo variable largely removes the correlations between M_* and other halo assembly properties, and the dependences of SFR, sSFR, and colour on halo assembly variables follow each other.

3.2.3 Dependence on M_{h} and V_{peak}

The correlations shown in Fig. 4 and Fig. 5 are for haloes of $\log[M_{\text{h}}/(h^{-1}M_{\odot})] \sim 12.0$ and $\log[V_{\text{peak}}/(\text{km s}^{-1})] \sim 2.23$. To obtain a full picture, in Fig. 6 we present the M_{h} and V_{peak} dependent Pearson correlation coefficients for the various pairs of galaxy and halo properties, by performing the calculation in different M_{h} and V_{peak} bins, respectively. The panels correspond to those in Fig. 4 and Fig. 5, and the correlation shown in a panel of a given row and column is between the property as labelled at the far left of the row and that at the bottom of the column. In each panel, the solid (dashed) curve is the dependence of ρ on M_{h} (V_{peak}), with zero correlation marked by the black dotted curve. Note that only V_{peak} is shown on the x -axis and the corresponding M_{h} can be obtained according to $M_{\text{h}} \propto V_{\text{peak}}^3$ from equation (1).

The panels with red curves show the correlations among halo properties. If we limit to halo properties other than M_{h} and V_{peak} , we find that the correlation of any pair of the assembly variables only weakly depends on M_{h} or V_{peak} if any (manifested by the nearly flat curves) and that the correlation strength does not depend on whether we use M_{h} or V_{peak} bins (manifested by the highly overlapped solid and dashed curves).

For the galaxy-halo correlations (in panels with black curves), in terms of M_{h} dependence, the strongest correlation between galaxy and halo property is found between M_* and $V_{\text{peak}}/c/a_{\text{M}/2}$ in low mass haloes, with $|\rho| \sim 0.5$ – 0.6 . It holds true in the full range of haloes considered here that using V_{peak} largely removes the correlation between M_* and any other halo assembly variable (dashed curves around zero). The only exception is that M_* appears to be slightly anti-correlated with c in low- V_{peak} haloes. With V_{peak} the dependences of correlation on V_{peak} for SFR, sSFR, and colour

² To see this, let $x = \log M_*$, $y = \log \text{SFR}$, and $z = \log \text{sSFR} = y - x$. We can derive the relation among the correlation coefficients, $\rho_{xz}/\rho_{yz} = (\rho_{xy} - \sigma_x/\sigma_y)/(1 - \rho_{xy}\sigma_x/\sigma_y)$. For ρ_{xz} to be near zero, we have $\rho_{xy} \sim \sigma_x/\sigma_y$.

closely track each other, which is not the case for those on M_h . With V_{peak} as the primary halo variable, star formation related properties (SFR, sSFR, and colour) mainly show dependence on halo formation time and then halo concentration.

For galaxy properties (in panels with blue curves), the correlation between SFR and M_* reaches a maximum in haloes of $\sim 10^{12} h^{-1} M_\odot$. It weakens in haloes of higher M_h or V_{peak} , probably because galaxies move away from the star-forming main sequence and passive evolution starts to dominate. However, the tight sSFR–SFR correlation persists over the full M_h or V_{peak} range. For colour, the correlation with SFR and sSFR is weak in low- M_h or low- V_{peak} haloes and becomes stronger in haloes of higher M_h or V_{peak} .

The results indicate that in the Illustris simulation galaxy formation ties to V_{peak} more closely than M_h . In comparison with the M_h -based results, we find that in terms of V_{peak} , galaxy properties show a cleaner trend in the correlation with other halo assembly variable, such as the lack of correlation for M_* and the similar correlation pattern for SFR/sSFR/colour. It suggests that V_{peak} -based halo model would be a good choice for capturing galaxy assembly bias effect (e.g. with M_* -based galaxy samples) and for studying galaxy assembly bias (e.g. with SFR/sSFR/colour-based samples). With V_{peak} as the primary halo variable in the model, halo formation time and concentration would be the main options for the secondary variable to describe the relation between halos and star formation related quantities, with the former preferable.

3.3 Assembly bias of central galaxies

With the set of galaxy and halo properties investigated in section 3.2, we do not find a galaxy property that 100 per cent correlates with a halo assembly property. For the M_h dependence, the strongest correlation has $|\rho| \sim 0.5\text{--}0.6$, between M_* and $V_{\text{peak}}/c/a_{M/2}$. It means that halo assembly bias cannot be fully inherited by galaxies and be fully translated to galaxy assembly bias. Galaxy assembly bias should be different from halo assembly bias. For example, for haloes of the same mass, we can split them into two halo samples of low and high concentrations and then split central galaxies into two galaxy samples with low and high M_* . There would be a difference in the clustering of the two halo samples, as well as in that of the two galaxy samples. Given that M_* is not perfectly correlated with c , we expect that the difference in the galaxy samples is smaller than that in the halo samples. As connecting galaxy assembly bias to halo assembly bias at the halo level can be an important ingredient in incorporating assembly bias effect into clustering model, we develop a simplified model below to understand the connection between galaxy and halo assembly bias.

Let us consider haloes at fixed M_h (or V_{peak}) and focus on one halo assembly variable x (e.g. $a_{M/2}$ or concentration) and one galaxy property y (e.g. M_* or SFR). Without losing generality, y is assumed to be positively correlated with x . The joint distribution of x and y is illustrated by an ellipse in the top panel of Fig. 7. We can form a halo sample by selecting the fraction f of haloes with the highest x (to the right of the vertical dashed line, the region inside the dashed curve) and a galaxy sample by selecting the same fraction of central galaxies with the highest y (above the red-purple

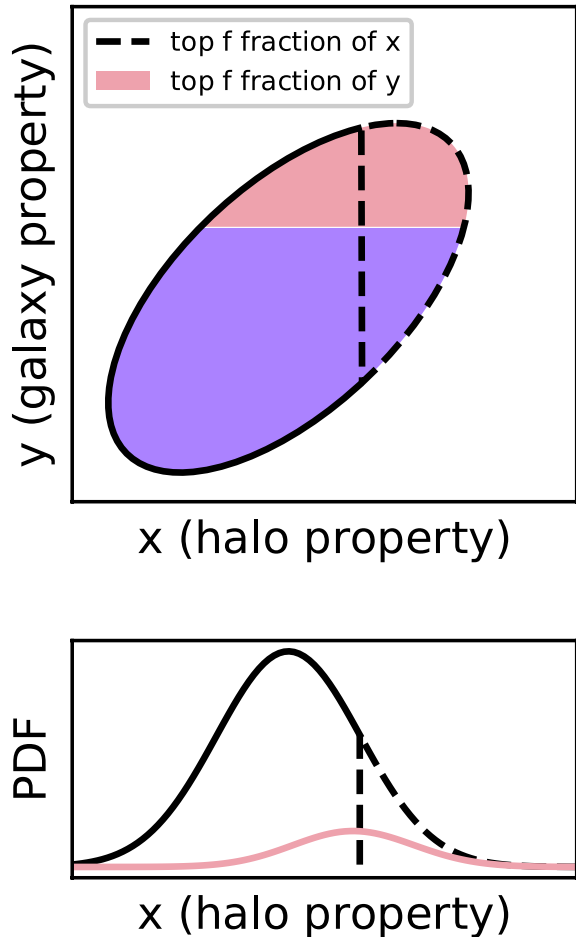


Figure 7. Illustration of the correlation between galaxy property and halo assembly property and the construction of the halo and galaxy samples for the study of galaxy assembly bias effect in section 3.3. In the top panel, the ellipse denotes the joint distribution of halo property x and galaxy property y at fixed M_h or V_{peak} , which is assumed to follow a 2D Gaussian distribution. A halo sample is constructed with haloes of the top f fraction of x (indicated by the red region), and a galaxy sample is constructed with central galaxies of the top f fraction of y (indicated by the region inside the dashed curve). Shown in the bottom panel are the probability distribution functions of halo property x for all the haloes at fixed M_h or V_{peak} (black solid+dashed), the selected haloes (dashed), and the selected galaxies (red solid), respectively.

dividing line, the region in red). Then, what is the relation between the bias factors of the galaxy and halo sample? To answer the question, in addition to $p(x, y)$, we also need the dependence of the halo bias factor $b(x, y)$ on x and y . For a sample G defined by cuts in galaxy property y or more generally cuts in the x - y plane, the corresponding bias factor

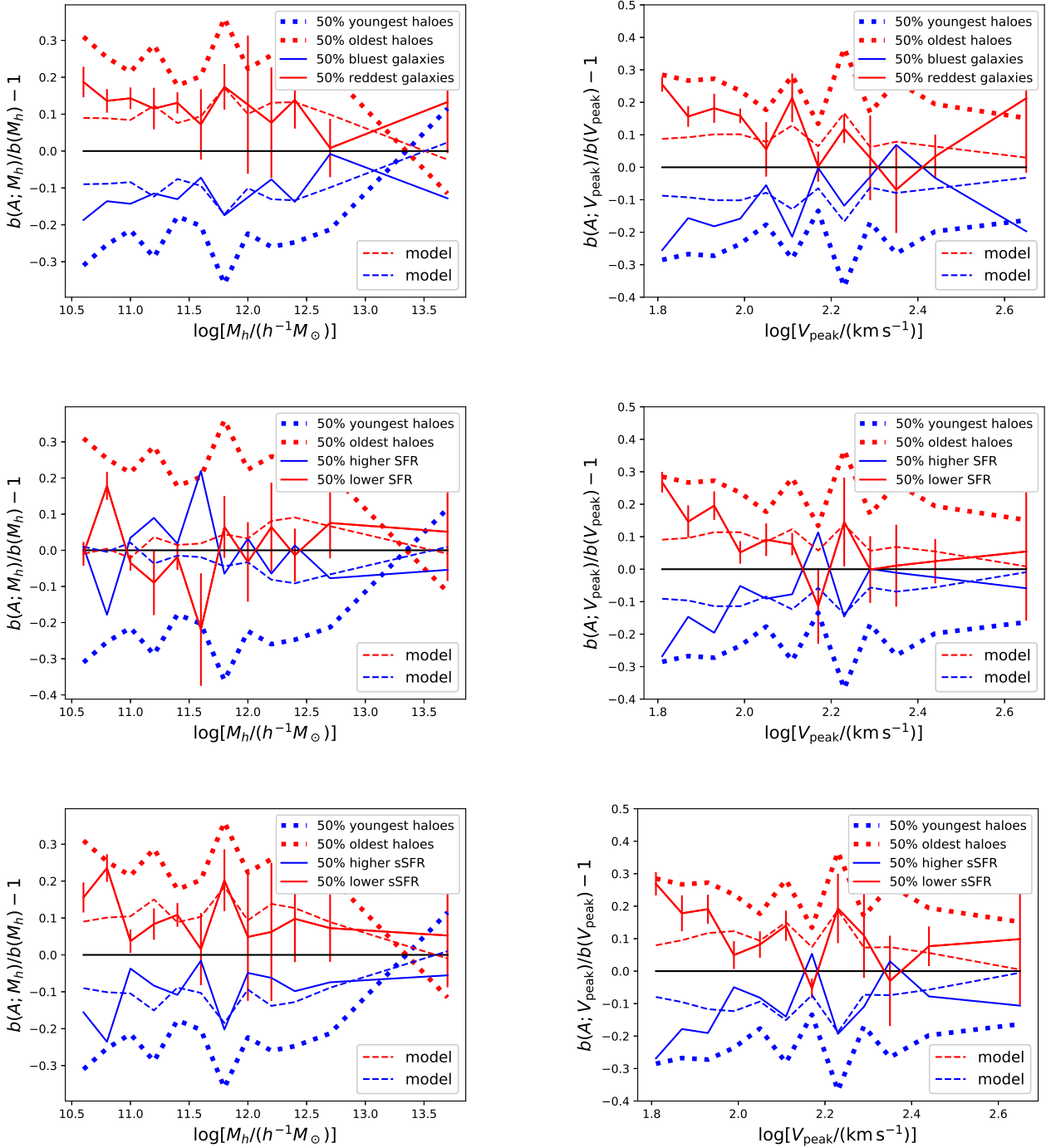


Figure 8. Connection between halo and galaxy assembly effect. In the left panels, the quantities shown are the values of $b(A, M_h)/b(M_h) - 1$ of different samples. For each sample, the quantity is the fractional difference of the bias factor of the sample selected based on property A with respect to that of all haloes at fixed M_h (i.e. δ_h^b or δ_g^b defined in section 3.3), which is used to characterise the magnitude of the assembly bias effect. The thick dotted curves are for halo samples selected based on halo formation time, and the solid curves are for central galaxy samples selected based on colour (top), SFR (middle), and sSFR (bottom). The thin dashed lines are the predictions from the simple model presented in section 3.3 according to the correlation between galaxy and halo properties ($\delta_g^b = \rho\delta_h^b$, with ρ the correlation coefficient). For clarity, jackknife error bars are only shown for the solid curves in each panel. The right panels are the same, but for the assembly bias effect as a function of V_{peak} . See details in section 3.3.

from haloes of fixed M_h or V_{peak} can be expressed as

$$b_G = \iint_G dx dy p(x, y) b(x, y), \quad (3)$$

where G indicates the region defined by the cuts.

To proceed, we make the following assumptions – (1) The joint distribution of galaxy and halo properties follows a 2-dimensional (2D) Gaussian $p(x, y)$, characterised by the centre (x_c, y_c) , standard deviations σ_x and σ_y , and the correlation ρ between x and y . We can take $(x_c, y_c) = (0, 0)$ by shifting x and y . A 2D Gaussian function is a reasonable approximation for the distributions seen in Fig. 4 and Fig. 5, which also follows the Taylor expansion of the logarithmic of the distribution function to the second order. (2) Galaxy property y has a strong dependence on the halo assembly property x , and only weakly on other halo assembly variables. That is, any galaxy assembly bias effect is a result of inheriting from the assembly bias effect in halo property x , not other halo assembly properties. With this assumption, $b(x, y)$ has no additional dependence other than x , simplifying to $b(x, y) = b(x)$. (3) At the fixed M_h (or V_{peak}), halo bias factor is linear with respect to halo property x , $b(x) = kx + b_c$, the first order approximation from Taylor expansion. The value b_c is the bias factor at $x = 0$, which is also the average halo bias factor for haloes at mass M_h (or V_{peak}). The slope k is the first derivative of b with respect to x , $k = \partial b / \partial x$. In Appendix B, we present and test an extension of the model by losing the assumptions (2) and (3), and the tests confirm that the simplification here is reasonable.

For the top f fraction of haloes with the highest x and that of galaxies with the highest y , the distribution of halo property x is shown in the bottom panel of Fig. 7 as the dashed curve and red curve, respectively. They are the projections of the region inside the dashed curve and that in red. Clearly the selected halo and galaxy samples differ in the mean halo property x , lower for the galaxy sample. The mean values can be calculated as

$$\langle x \rangle_{x > t\sigma_x} = \frac{\int_{t\sigma_x}^{+\infty} dx \int_{-\infty}^{+\infty} dy x p(x, y)}{\int_{t\sigma_x}^{+\infty} dx \int_{-\infty}^{+\infty} dy p(x, y)} = \frac{\sigma_x \exp(-t^2/2)}{\int_t^{+\infty} dv \exp(-v^2/2)} \quad (4)$$

and

$$\langle x \rangle_{y > t\sigma_y} = \frac{\int_{t\sigma_y}^{+\infty} dy \int_{-\infty}^{+\infty} dx x p(x, y)}{\int_{t\sigma_y}^{+\infty} dy \int_{-\infty}^{+\infty} dx p(x, y)} = \frac{\rho \sigma_x \exp(-t^2/2)}{\int_t^{+\infty} dv \exp(-v^2/2)}, \quad (5)$$

where t is determined by having the correct fraction f ,

$$f = \int_t^{+\infty} dv \frac{1}{\sqrt{2\pi}} \exp(-v^2/2). \quad (6)$$

The bias factors for the halo and galaxy samples are then

$$b_h = \langle b \rangle_{x > t\sigma_x} = k \langle x \rangle_{x > t\sigma_x} + b_c \quad (7)$$

and

$$b_g = \langle b \rangle_{y > t\sigma_y} = k \langle x \rangle_{y > t\sigma_y} + b_c. \quad (8)$$

We can characterise the assembly bias effect by the fractional difference between the bias factor of the selected halo/galaxy sample and the average halo bias factor at M_h (or V_{peak}), $\delta_h^b = (b_h - b_c) / b_c$ and $\delta_g^b = (b_g - b_c) / b_c$. Based on equations (4)–(8), we have

$$\delta_g^b = \rho \delta_h^b. \quad (9)$$

That is, the assembly bias effect of the galaxy sample is weaker than that of the halo sample, by a factor equal to the correlation coefficient of the galaxy and halo property. Only in the case that galaxy and halo properties are tightly correlated (with zero scatter; $|\rho| = 1$) does halo assembly bias effect completely translate to galaxy assembly bias effect. The connection in equation (9) is also valid for samples defined by the property range bounded by two percentiles (i.e. bin samples rather than threshold samples considered here).

To test how well the simple model works, we choose a pair of halo and galaxy properties to construct the halo and galaxy samples. We then measure the two-point correlation functions (2PCFs) of the halo and galaxy samples in each M_h and V_{peak} bin. To reduce the uncertainty, the large scale bias factor of a given halo sample is derived from the ratio of the halo-matter two-point cross-correlation function and the matter auto-correlation function (e.g. Xu & Zheng 2018), $b_h = \xi_{hm}(r) / \xi_{mm}(r)$, averaged over scales of 5–18 h^{-1} Mpc. The bias factor for the galaxy sample is similarly derived. We consider samples based on halo formation time $a_{M/2}$ and galaxy colour/SFR/sSFR, which show M_h (V_{peak}) dependent correlation coefficient (Fig. 6). The results are shown in Fig. 8. In the top-left panel, the thick dotted red (blue) curves show the assembly bias quantity δ_h^b for the 50 per cent oldest (youngest) haloes as a function of M_h . The solid red (blue) curves are δ_g^b for the 50 per cent reddest (bluest) central galaxies. Both quantities decrease with increasing halo mass, i.e. the assembly bias effect becomes weaker for more massive haloes. The thin dashed curves are the same as the dotted curves but modulated by the correlation coefficient between colour and $a_{M/2}$, i.e. $\rho \delta_h^b$, the prediction for δ_g^b from the simple model. The model works well in reproducing the halo mass dependent galaxy assembly bias effect based on halo assembly bias and the galaxy-halo correlation. The middle-left and bottom-left panels are for galaxies selected according to SFR and sSFR. The right panels show the assembly bias effect as a function of V_{peak} . In all the cases, δ_g^b can be well described by $\rho \delta_h^b$, which supports the effectiveness of the simple model.

The success of the model suggests that an easy recipe could be developed to incorporate galaxy assembly bias into the halo model. The contribution of central galaxies to the galaxy bias factor, in its full form in the simple model, is

$$b_g = b_c + \frac{\partial b}{\partial x} \left[x_c + \sigma_x \frac{\rho}{\sqrt{2\pi}} \exp(-t^2/2) / f \right], \quad (10)$$

where $t = t(f)$ is from equation (6). As an example, let us use the halo mass M_h as the primary variable in the halo model and consider a galaxy property (colour) that correlates with halo formation time ($a_{M/2}$ or $\log a_{M/2}$). In the halo model, besides the average halo bias b_c , we also need to know how the halo bias changes with $a_{M/2}$ ($\partial b / \partial x$), the mean value of $a_{M/2}$ (x_c), and the scatter in $a_{M/2}$ (σ_x), all as a function of M_h . As usual, we can construct fitting formulae for those four quantities based on N -body simulations. The quantities f and ρ belong to the description of the galaxy-halo relation, which can be parameterised. For f , it is simply the occupation fraction for haloes at M_h . For ρ , the results in Fig. 6 suggest that a quadratic form with M_h would suffice. To compute the galaxy bias factor for a galaxy sample, we only need to perform a 1D integral over halo mass. Certainly

it is straightforward to include assembly bias effect by populating dark matter haloes in N -body simulations. However, the above proposal has its virtue for analytic calculations in theoretical investigations.

The simple model can also be applied to observation to infer the correlation between galaxy and halo properties. Lin et al. (2016) construct samples of central galaxies from the Sloan Digital Sky Survey data and study the assembly bias effect from the 2PCF measurements. Early and late galaxy samples are defined according to either star formation history (SFH) or sSFR. Weak lensing measurements are used to verify that the host haloes of the early and late galaxies are of similar halo mass (around $10^{12}h^{-1}M_{\odot}$). Lin et al. (2016) compare the difference in the early and late galaxy clustering to that in the early and late formed haloes, and do not find evidence for galaxy assembly bias. For SFH-based galaxy samples, they find the ratio of the early to late galaxy bias factor to be 1.00 ± 0.12 (see their fig.5). If we take the mean of the bias factors of the two galaxy samples as the average halo bias and the uncertainty comes from two similar error bars added in quadrature, the measurement gives $\delta_g^b = 0$ with an uncertainty 0.085. For halos around $10^{12}h^{-1}M_{\odot}$, $\delta_h^b \sim 0.25$, with early- and late-forming haloes (Fig. 6). The coefficient of the correlation between SFH and halo formation time is then inferred to be $\rho = \delta_g^b/\delta_h^b = 0.00 \pm 0.34$. For the sSFR-based samples, the ratio of the early to late galaxy bias factor is 1.07 ± 0.14 (their fig.5). We infer $\delta_g^b = 0.034 \pm 0.099$, and with $\delta_h^b \sim 0.25$ the coefficient of the correlation between sSFR and halo formation time is constrained to be $\rho = 0.14 \pm 0.40$. For both cases, the correlation between galaxy and halo property is consistent with being small. It implies that galaxy SFH and sSFR at most only loosely track halo formation. Similar measurements with large samples can reduce the uncertainty in the inferred correlation, which would help test galaxy formation models (e.g. by comparing to those in Fig. 6).

4 SUMMARY AND DISCUSSION

Properties in galaxies residing in haloes of the same mass may have a dependence on certain aspects of halo assembly or formation history, which is termed as galaxy assembly bias. Studying galaxy assembly bias and its relation to halo properties can help improve the halo model of galaxy clustering and yield insights in galaxy formation and evolution. Using the Illustris cosmological hydrodynamic galaxy formation simulation, we investigate the central galaxy assembly bias effect through studying the relation among a set of galaxy and halo properties.

The main results can be summarised as follows.

- (1) Central galaxy stellar mass M_* has a tighter relation with V_{peak} than with M_h , manifested by the smaller scatter in M_* at fixed V_{peak} than that at fixed M_h . Once the assembly effect of M_* on V_{peak} is included, M_* shows nearly no correlation with any other halo assembly properties.
- (2) The correlations between halo assembly properties and other galaxy properties also appear cleaner if studied at fixed V_{peak} , which reveal that galaxy SFR, sSFR, and colour mainly correlate with halo formation time (and to a less extent with halo concentration).
- (3) A simple model is presented to show the relation be-

tween galaxy and halo assembly bias, which is linked by the correlation coefficient of the galaxy and halo property in consideration.

The Illustris simulation produces a relation between central galaxy stellar mass and halo mass (M_*-M_h) similar to that inferred from observation. We find that the scatter in the relation is closely related to halo assembly properties. For example, at fixed M_h , haloes of higher V_{peak} or earlier formation tend to host galaxies of higher M_* . If we choose V_{peak} to be the primary halo variable, the scatter in M_* at fixed V_{peak} is reduced compared to that at fixed M_h . Remarkably, once switched to V_{peak} , M_* appears to have nearly no dependence on other halo assembly properties, at least for those considered in our study (including halo concentration, formation time, spin, accretion rate, and specific accretion rate). The property V_{peak} , which is an indication of the maximum potential depth over the assembly history of haloes, is able to capture almost all the assembly effect in galaxy stellar mass. The results are in broad agreement with the study using the EAGLE simulation in terms of the $z = 0$ maximum halo circular velocity (Matthee et al. 2017). The reason for V_{peak} to be the fundamental property in determining M_* is likely related to the accretion and response of baryons in the gravitational potential. As for the scatter, the simulation noise in Illustris does not contribute much (Genel et al. 2019). It could be related to chaotic or stochastic processes in star formation and feedback (Matthee et al. 2017; Genel et al. 2019). Further study is needed to understand the cause of the correlation between M_* and V_{peak} and the origin of the scatter.

We present the correlation between each pair of galaxy and halo property in terms of the Pearson correlation coefficient. Besides M_* , the other galaxy properties (SFR, sSFR, and colour) show a more consistent and clear trend with V_{peak} than with M_h . At fixed V_{peak} , those other galaxy properties related to star formation are found to mainly correlate with halo formation time and concentration, with stronger correlation with the former. The relatively nice behaviour in the correlations with galaxy properties in the V_{peak} -based investigation suggests that it would be advantageous to use V_{peak} as the primary variable in halo model of galaxy clustering, in particular in modelling stellar-mass-based samples (while the combination of or interpolation between halo mass and circular velocity quantities remains as a possibility to investigate, in the spirit of Lehmann, Mao, Becker, Skillman & Wechsler 2017). To further model SFR-, sSFR-, or colour-selected samples of galaxies, our investigation suggests to introduce *halo formation time as the secondary halo variable* (and to a less extent, halo concentration). This is in line with the age-matching model of Hearin & Watson (2013), who assumes monotonic mapping between galaxy colour and some variant of halo formation time at fixed galaxy luminosity (or stellar mass). That is, there exists a perfect correlation between the galaxy and halo property. Our investigation shows, however, that the correlation coefficient between galaxy SFR/sSFR/colour and halo formation time should be included as one important ingredient in the model.

The Illustris simulation is able to reproduce the observed star-forming main sequence reasonably well (Sparre et al. 2015). Here we find that at fixed M_h or V_{peak} the rela-

tion between SFR and M_* of central galaxies follows the star-forming main sequence. Interestingly, compared with the SFR– M_* relation, SFR shows a tighter correlation with sSFR ($\rho \sim 0.9$) over the full halo M_h or V_{peak} range. It is necessary to test its validity with observations and study its origin by tracking SFR and stellar mass growth of individual galaxies in simulations. The correlation between SFR and sSFR or between any pair of galaxy properties (M_* , SFR, sSFR, and colour) considered here cannot be explained solely by their common dependence on one halo assembly variable. Baryonic processes in galaxy formation (like star formation and feedback) likely play a major role in shaping such correlations.

For the effect of assembly bias on galaxy clustering, at fixed M_h or V_{peak} , we come up with a simple model to relate the bias factors of a galaxy sample and the corresponding halo sample, which are connected by the correlation coefficient of the galaxy and halo properties used to define the two samples. It gives a reasonable description for the samples constructed with the simulation. It suggests a simple prescription to incorporate galaxy assembly bias into the halo model. By applying the simple model to the galaxy clustering measurements in [Lin et al. \(2016\)](#), we infer that the correlation between SFH/sSFR and halo formation time is consistent with being weak ($\rho \sim 0\text{--}0.14$). The simple model can be further tested with other hydrodynamic simulations, like EAGLE ([Schaye et al. 2015](#)) and IllustrisTNG ([Nelson et al. 2019](#)), and semi-analytic models, which can also provide further insights on parameterising the correlations between galaxy and halo properties. While our study in this paper focuses on central galaxies, we plan to carry out similar investigations for satellite galaxies to complete the picture of galaxy assembly bias at the halo level to help improve the halo model.

ACKNOWLEDGEMENTS

We thank David Weinberg, Jeremy Tinker and Hélión du Mas des Bourboux for useful comments. The support and resources from the Center for High Performance Computing at the University of Utah are gratefully acknowledged. This research was supported by the Munich Institute for Astro- and Particle Physics (MIAPP) of the DFG cluster of excellence “Origin and Structure of the Universe”, and ZZ thanks the hospitality of MIAPP, where the revision of the manuscript was undertaken.

REFERENCES

- Artale M. C., Zehavi I., Contreras S., & Norberg P. 2018, MNRAS, 480, 3978
- Bardden J. M., Bond J. R., Kaiser N., & Szalay A. S. 1986, ApJ, 304, 15
- Behroozi P. S., Conroy C., & Wechsler R. H. 2010, ApJ, 717, 379
- Behroozi P. S., Wechsler R. H., & Wu H.-Y. 2013, ApJ, 762, 109
- Behroozi P. S., Wechsler R. H., Wu H.-Y., et al. 2013, ApJ, 763, 18
- Berlind A. A., & Weinberg D. H. 2002, ApJ, 575, 587
- Berlind, A. A., Weinberg, D. H., Benson, A. J., et al. 2003, ApJ, 593, 1
- Berlind, A. A., Kazin, E., Blanton, M. R., et al. 2006, arXiv:astro-ph/0610524
- Bose S., Eisenstein D. J., Hernquist I., et al. 2019, MNRAS, 490, 5693
- Brinchmann J., Charlot S., White S. D. M., Tremonti C., Kauffmann G., Heckman T., Brinkmann J., 2004, MNRAS, 351, 1151
- Castorina E., Sheth R. K. 2013, MNRAS, 433, 1529
- Chaves-Montero J., Angulo R. E., Schaye J., et al. 2016, MNRAS, 460, 3100
- Contreras S., Zehavi I., Padilla N., et al. 2019, MNRAS, 484, 1133
- Cooray A., & Sheth R. 2002, Phys. Rept., 372, 1
- Croton, D. J., Gao, L., & White, S. D. M. 2007, MNRAS, 374, 1303
- Dalal N., White M., Bond J. R., & Shirokov A. 2008, ApJ, 687, 12
- Gao L., Springel V., & White S. D. M. 2005, MNRAS, 363, L66
- Gao L., & White S. D. M. 2007, MNRAS, 377, L5
- Genel S., et al., 2014, MNRAS, 445, 175
- Genel S., et al., 2019, ApJ, 871, 21
- Gu M., Conroy C., & Behroozi P. 2016, ApJ, 833, 2
- Guo H., et al., 2016, MNRAS, 459, 3040
- Guo H., Li C., Zheng Z., et al. 2017, ApJ, 846, 61
- Han J., Li Y., Jing Y. P., Nishimichi T., Wang W., & Jiang C. 2019, MNRAS, 482, 1900
- Hearin A. P., Watson D. F., 2013, MNRAS, 435, 1313
- Jeeson-Daniel, A., Dalla Vecchia, C., Haas, M. R., et al. 2011, MNRAS, 415, L69.
- Leauthaud A., Tinker J., Bundy K., et al. 2012, ApJ, 744, 159
- Lehmann B. V., Mao Y.-Y., Becker M. R., Skillman S. W., Wechsler R. H., 2017, ApJ, 834, 37
- Lin Y.-T., Mandelbaum R., Huang Y.-H., et al. 2016, ApJ, 819, 119
- Mao Y.-Y., Zentner A. R., Wechsler R. H., 2018, MNRAS, 474, 5143
- Mansfield P., & Kravtsov A. V. 2019, arXiv:1902.00030
- Martizzi D., Vogelsberger M., Torrey P., et al. 2019, arXiv:1907.04333
- Matthee J., Schaye J., Crain R. A., Schaller M., Bower R., Theuns T., 2017, MNRAS, 465, 2381
- McCarthy K. S., Zheng Z., Guo H., 2019, MNRAS, 487, 2424
- McEwen J. E., Weinberg D. H., 2016, arXiv e-prints, arXiv:1601.02693
- Mehta, K. T. 2014, Ph.D. Thesis,
- Mo H. J., & White S. D. M. 1996, MNRAS, 282, 347
- Nelson D., et al., 2015, A&C, 13, 12
- Nelson D., et al., 2019, A&C, 6, 2
- Paranjape A., Hahn O., & Sheth R. K. 2018, MNRAS, 476, 3631
- Press W. H., & Schechter P. 1974, ApJ, 187, 425
- Prada F., Klypin A. A., Cuesta A. J., Betancort-Rijo J. E., & Primack J. 2012, MNRAS, 423, 3018
- Ramakrishnan S., Paranjape A., Hahn O., & Sheth R. K. 2019, MNRAS, 489, 2977
- Reddick R. M., Wechsler R. H., Tinker J. L., & Behroozi P. S. 2013, ApJ, 771, 30
- Santini P., et al., 2017, ApJ, 847, 76
- Schaye J., Crain R. A., Bower R. G., et al. 2015, MNRAS, 446, 521
- Sheth R. K., & Tormen G. 1999, MNRAS, 308, 119
- Shi J., & Sheth R. K. 2018, MNRAS, 473, 2486
- Sparre M., et al., 2015, MNRAS, 447, 3548
- Speagle J. S., Steinhardt C. L., Capak P. L., Silverman J. D., 2014, ApJS, 214, 15
- Springel V., White S. D. M., Jenkins A., et al. 2005, NATURE, 435, 629
- Tinker J. L., et al., 2017, ApJ, 839, 121
- Tinker, J. L. 2017, MNRAS, 467, 3533.
- Villarreal A. S., Zentner S. R., Mao Y., et al. 2017, MNRAS, 472, 1088

- Vogelsberger M., Genel S., Springel V., et al. 2014, MNRAS, 444, 1518
- Vogelsberger M., Genel S., Springel V., et al. 2014, NATURE, 509, 177
- White S. D. M., Rees M. J. 1978, MNRAS, 183, 341
- Xu H., Zheng Z., Guo H., Zu Y., Zehavi I., & Weinberg D. H. 2018, MNRAS, 481, 5470
- Xu X., & Zheng Z. 2018, MNRAS, 479, 1579
- Yang X., Mo H. J., & van den Bosch F. C. 2003, MNRAS, 339, 1057
- Yang X., Mo H. J., & van den Bosch F. C. 2006, ApJ, 638, L55
- Zehavi I., Zheng Z., Weinberg D. H., et al. 2005, ApJ, 630, 1
- Zehavi I., Contreras S., Padilla N., et al. 2018, ApJ, 853, 84
- Zehavi I., Kerby S. E., Contreras S., et al. 2019, ApJ, 887, 17
- Zentner A. R., Hearin A. P., & van den Bosch F. C. 2014, MNRAS, 443, 3044
- Zentner, A. R., Hearin, A., van den Bosch, F. C., Lange, J. U., & Villarreal, A. 2019, MNRAS, 485, 1196
- Zheng Z., Berlind A. A., Weinberg D. H., et al. 2005, ApJ, 633, 791
- Zheng Z., Coil A. L., & Zehavi I. 2007. ApJ, 667, 760
- Zu Y., Zheng Z., Zhu G., Jing Y. P., 2008, ApJ, 686, 41
- Zu Y., & Mandelbaum R. 2015, MNRAS, 454, 1161
- Zu Y., Mandelbaum R., Simet M., Rozo E., & Rykoff E. S. 2017, MNRAS, 470, 551

APPENDIX A: THE M_* - V_{max} RELATION AND THE BARYON EFFECT ON THE M_* - V_{peak} RELATION

In section 3.1, we show that central galaxy M_* has a tight correlation with V_{peak} and there is no further dependence on $a_{M/2}$ at fixed V_{peak} . The other velocity quantity commonly considered is V_{max} , the present-day maximum circular velocity of a halo. While both V_{peak} and V_{max} characterise the depth of the potential well of a halo, the computation of V_{max} in a simulation is more straightforward, without tracking the whole formation history of a halo. We find that the M_* - V_{max} relation is similar to the M_* - V_{peak} relation, as shown in the left panel of Fig. A1. However, the M_* - V_{max} relation has a residual dependence on $a_{M/2}$, with on average higher stellar mass in older haloes. This suggests that V_{peak} better captures the effect of halo formation time on the final central galaxy stellar mass than V_{max} .

In the right panel of Fig. A1, we show the standard deviation in $\log M_*$ as a function of V_{peak} and V_{max} , respectively. We fit a straight line to derive the mean relation between $\log V_{\text{peak}}$ and $\log V_{\text{max}}$, and the correspondence between V_{peak} and V_{max} in the figure comes from such a fit. The V_{max} dependence of the scatter in M_* only slightly differs from the V_{peak} dependence. In particular, compared to the V_{peak} dependence of the scatter in M_* , that for the V_{max} dependence is smaller (higher) for haloes with V_{peak} below (above) $\sim 300 \text{ km s}^{-1}$. Although V_{peak} explains the dependence of M_* on formation time better than V_{max} , the tighter M_* - V_{max} relation in lower V_{peak} haloes indicates that M_* could also depend on variables other than halo formation time (e.g. halo environment).

In section 3.1, the quantity V_{peak} used in the analyses is from the full physics simulation of Illustris. One may wonder whether baryons are partly responsible for the tight M_* - V_{peak} relation, as gas cooling with subsequent star formation can deepen the potential and thus change V_{peak} . We explore the baryon effect on the M_* - V_{peak} relation by replacing V_{peak} and

$a_{M/2}$ with those in the dark-matter-only (DMO) simulation, after matching Rockstar haloes found in the Illustris-2-Dark simulation to those in the Illustris-2 simulation. In the left panel of Fig. A2, we show the ratio of full physics (hydro) V_{peak} to the DMO V_{peak} as a function of DMO V_{peak} . At each DMO V_{peak} bin, we further divide haloes into two halves, with high and low M_* , respectively. Haloes with more massive central galaxies at fixed DMO V_{peak} tend to have higher hydro-to-DMO V_{peak} ratio, reflecting the effect of baryons on deepening the potential. The difference between hydro V_{peak} and DMO V_{peak} is larger in haloes of lower DMO V_{peak} . However, the overall difference is small, e.g. below ~ 3 per cent. This difference plays a negligible role in the M_* - V_{peak} relation, as shown by comparing the right panel of Fig. A2 to the bottom-right panel of Fig. 1.

APPENDIX B: A MORE GENERAL FORM OF CENTRAL GALAXY ASSEMBLY BIAS

In section 3.3 we develop a simple model to describe central galaxy assembly bias based on halo assembly bias and galaxy-halo relation. In that model, bias is assumed to depend only on one halo property at fixed halo mass. The model works reasonably well based on the tests with Illustris simulation. Since halo assembly bias is found to have a multi-variate dependence (e.g. Mao, Zentner & Wechsler 2018; Xu & Zheng 2018; Han et al. 2019), it is useful to extend the simple model for more general applications. Instead of increasing the dimensionality of the model and describing halo assembly bias as a function of multiple halo assembly variables at fixed halo mass, we choose to model halo bias as a function of one halo assembly property (x) and one galaxy property (y). That is, the bias dependence on any additional halo assembly properties is absorbed into that on the galaxy property (as galaxy property can be related to those halo properties). Additionally, the bias factor is assumed to be linearly dependent on halo and galaxy property, $b(x, y) = k_x x + k_y y + b_c$. Therefore, the contours of constant bias now have the possibility of deviating from vertical in the top panel of Fig. 7. The coefficient k_y captures the dependence of y on other halo properties and the scatter in the y - x relation.

With this model, equations (7) and (8) become

$$b_h = \langle b \rangle_{x > t\sigma_x} = k_x \langle x \rangle_{x > t\sigma_x} + k_y \langle y \rangle_{x > t\sigma_x} + b_c \quad (\text{B1})$$

and

$$b_g = \langle b \rangle_{y > t\sigma_y} = k_x \langle x \rangle_{y > t\sigma_y} + k_y \langle y \rangle_{y > t\sigma_y} + b_c, \quad (\text{B2})$$

where the new terms $\langle x \rangle_{x > t\sigma_x}$ and $\langle y \rangle_{y > t\sigma_y}$ can be calculated as

$$\langle y \rangle_{x > t\sigma_x} = \frac{\int_{t\sigma_x}^{+\infty} dx \int_{-\infty}^{+\infty} dy y p(x, y)}{\int_{t\sigma_x}^{+\infty} dx \int_{-\infty}^{+\infty} dy p(x, y)} = \frac{\rho \sigma_y \exp(-t^2/2)}{\int_t^{+\infty} dv \exp(-v^2/2)} \quad (\text{B3})$$

and

$$\langle y \rangle_{y > t\sigma_y} = \frac{\int_{t\sigma_y}^{+\infty} dy \int_{-\infty}^{+\infty} dx y p(x, y)}{\int_{t\sigma_y}^{+\infty} dy \int_{-\infty}^{+\infty} dx p(x, y)} = \frac{\sigma_y \exp(-t^2/2)}{\int_t^{+\infty} dv \exp(-v^2/2)}. \quad (\text{B4})$$

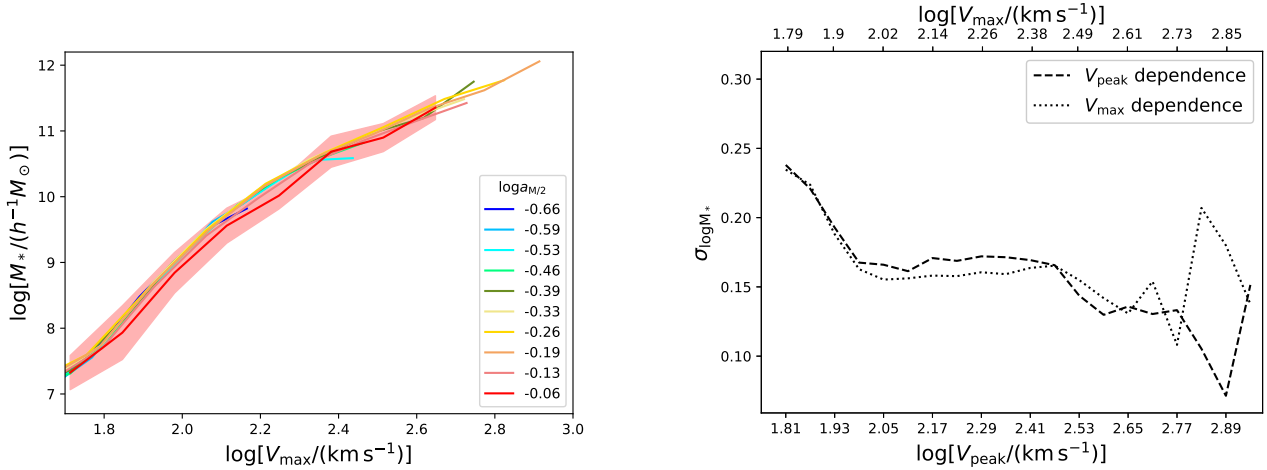


Figure A1. Left: Same as the bottom-right panel of Fig. 1, but showing the dependence of M_* on V_{\max} instead of V_{peak} . Right: Similar to Fig. 2, but comparing the standard deviations in $\log M_*$ as a function of V_{peak} and V_{\max} . The correspondence between V_{peak} and V_{\max} comes from fitting a mean relation (see text for detail).

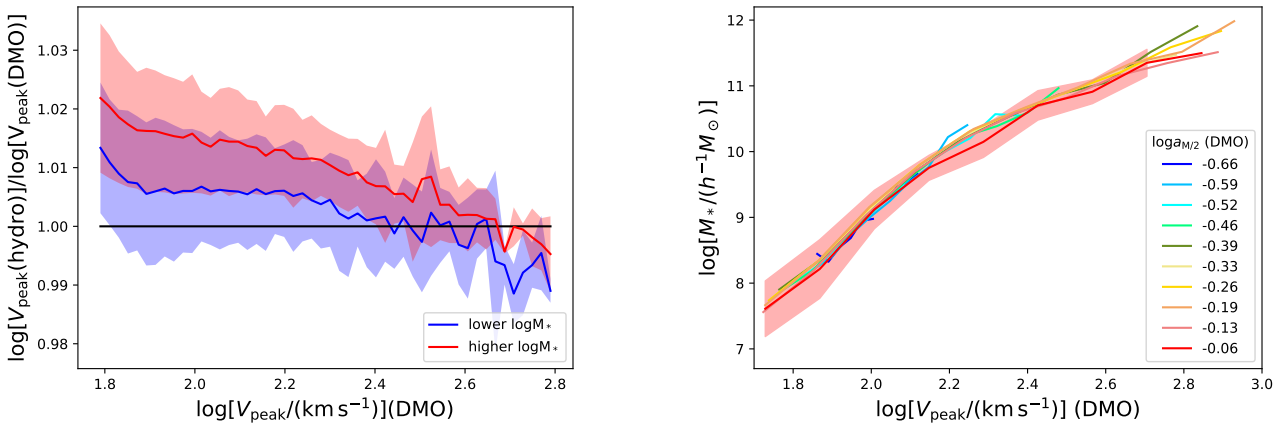


Figure A2. Effect of baryonic physics on V_{peak} . Left: ratio of V_{peak} from the full physics (hydro) simulation to that from the DMO simulation as function of DMO V_{peak} . Red and blue solid are V_{peak} ratio for haloes with central stellar mass in the upper and lower halves at fixed DMO V_{peak} . Standard deviations are shown by red and blue bands. Note that hydro V_{peak} only slightly differ from DMO V_{peak} , at the per cent level. Right: similar to the bottom-right panel of Fig. 1, but with V_{peak} and $a_{M/2}$ from the DMO simulation.

Similar to what we do in section 3.3 and based on equations (B3), (B4), (B1), (B2), (4), and (5), we obtain the following relation between the fractional halo and galaxy assembly bias (δ_h^b and δ_g^b),

$$\delta_g^b = \frac{\rho + \gamma}{1 + \rho\gamma} \delta_h^b, \quad (\text{B5})$$

where $\gamma = (k_y\sigma_y)/(k_x\sigma_x)$ is an indicator of the relative importance of the bias dependence on galaxy and halo property. For $\gamma=0$ (e.g. with $k_y = 0$), this model reduces to the simple one in section 3.3, with the bias gradient along the x direction (bias contours being vertical). In general, $|\gamma| < |\rho|$ corresponds to bias contours close to vertical, while $|\gamma| > |\rho|$ close to horizontal. In the following we will investigate which case represents that in the simulation by calculating γ .

We examine the performance of equation (B5) using the Illustris simulation and test the importance of γ . Same

as in section 3.3, halo assembly property (x) we consider is the formation time $a_{M/2}$, and galaxy properties (y) include colour, SFR, and sSFR. At a fixed M_h or V_{peak} bin, haloes are divided into four sub-samples, depending which lower/upper halves of x and lower/upper halves of y they belong to. We measure the bias factors of the sub-samples and derive k_x and k_y from fitting them with $b = k_x\langle x \rangle + k_y\langle y \rangle + b_c$. Together with the measured standard deviations σ_x and σ_y , we infer γ in equation (B5).

The results are shown in Fig. B1. It is similar to Fig. 8, except that a set of dash-dotted curves are added to show the predicted δ_g^b by equation (B5) (and that larger bins are used for haloes of high M_h/V_{peak} to reduce the noise in the bias measurements for sub-samples). Clearly the more general model of equation (B5) leads to better agreements with the measured galaxy assembly bias, and in almost of the cases the predictions just fall on top of the measurements. In general, however, we find that γ only plays a minor role

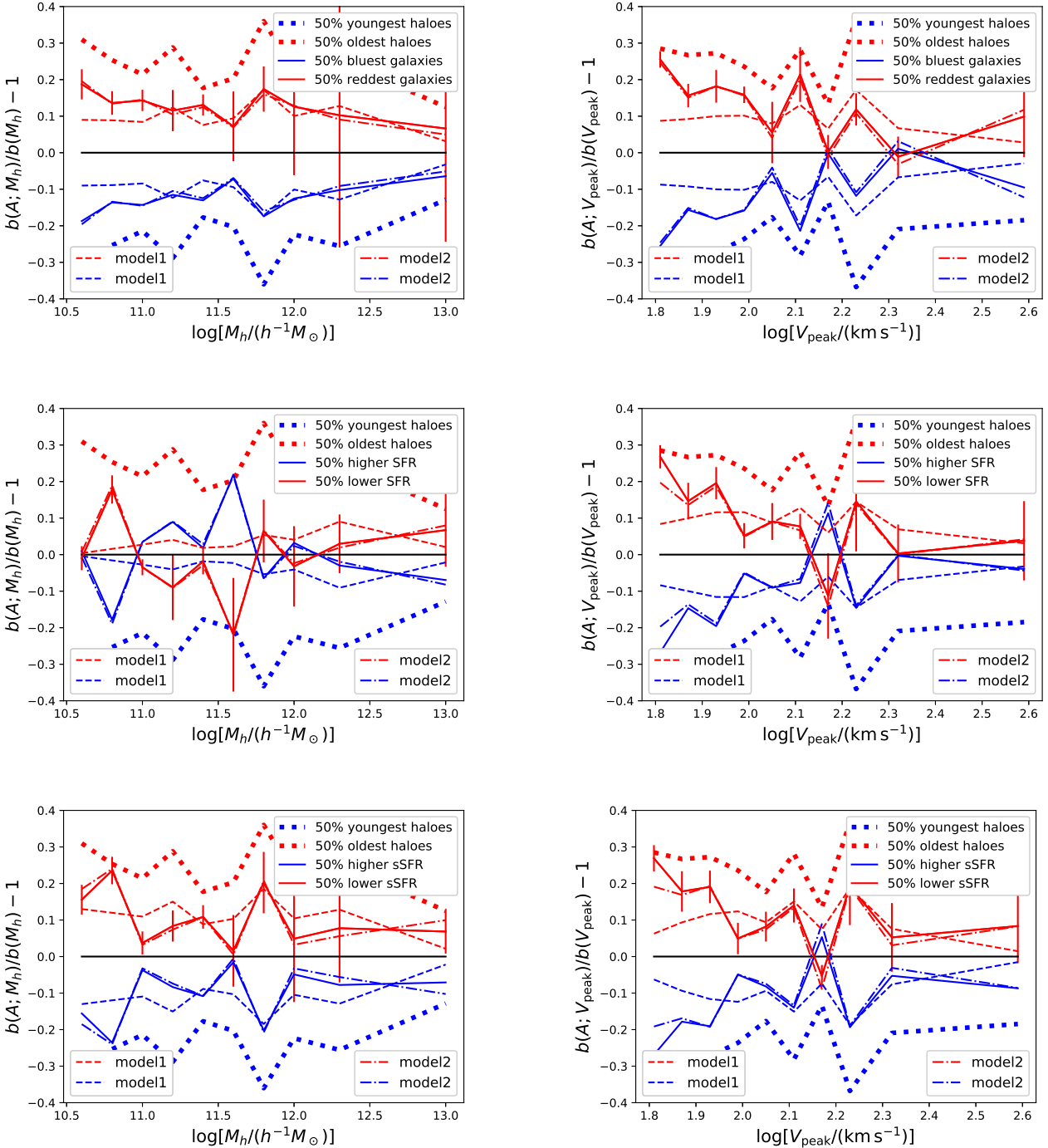


Figure B1. Same as Fig. 8, but in comparison to the predictions from the simple model (dashed, labelled as ‘model 1’) in section 3.3, those from a more general model (dash-dotted, labelled as ‘model 2’) are added. See text for detail.

in determining the fractional assembly bias, compared to ρ . For example, we find $\gamma = -0.13 \pm 0.22$ with $a_{M/2}$ and galaxy colour across all M_h bins, lower in amplitude than ρ (about 0.3–0.5, as shown in Fig. 6). Similar results are also obtained with other galaxy properties that we used in Fig. 8. That is, as long as the halo assembly property we identify is closely connected to galaxy property, any additional dependence of bias (on other halo properties, through that on galaxy prop-

erty) is weak. The result indicates that considering only the bias dependence of such a halo property is sufficient to describe the most useful part of halo bias in modelling galaxy bias and the simple model in section 3.3 would work reasonably well. It would be interesting to see how general this holds by testing with more galaxy and halo properties and by using different galaxy formation simulations.

If one would like to incorporate any additional bias de-

pendence into the model, the counterpart of equation (10) for the contribution of central galaxies to the galaxy bias factor reads

$$b_g = b_c + \frac{\partial b}{\partial x} \left[x_c + \Delta x_c + \sigma_x \frac{\rho_{\text{eff}}}{\sqrt{2\pi}} \exp(-t^2/2)/f \right], \quad (\text{B6})$$

where $\Delta x_c = \gamma(\sigma_x/\sigma_y)y_c$ and $\rho_{\text{eff}} = \rho + \gamma$. Instead of parameterising ρ (as a function of M_h), we now only need to describe two quantities, the offset Δx_c in halo assembly property and the effective correlation coefficient ρ_{eff} . As with equation (10), the expression follows the spirit of halo model – b_c , $\partial b/\partial x$, x_c , and σ_x are halo properties, while Δx_c , ρ_{eff} , t , and f describe the galaxy-halo relation, which includes the correlation and scatter between the galaxy and halo property and the galaxy occupation function.

To achieve more precise modelling, it is also possible to express halo bias as linear functions of more than two halo properties, instead of absorbing that into the dependence of galaxy property, and to include quadratic dependence of each halo property. While such extensions are straightforward in our framework, it requires multi-variate descriptions of halo and galaxy properties with a substantially increased number of parameters, making the model less tractable and less attractive. In practice, the simple model presented in section 3.3 would be a useful first step.

This paper has been typeset from a $\text{T}_{\text{E}}\text{X}/\text{L}^{\text{A}}\text{T}_{\text{E}}\text{X}$ file prepared by the author.